

# Progressive Joint Low-light Enhancement and Noise Removal for Raw Images

Yucheng Lu and Seung-Won Jung, *Senior Member, IEEE*

**Abstract**—Low-light imaging on mobile devices is typically challenging due to insufficient incident light coming through the relatively small aperture, resulting in a low signal-to-noise ratio. Most of the previous works on low-light image processing focus either only on a single task such as illumination adjustment, color enhancement, or noise removal; or on a joint illumination adjustment and denoising task that heavily relies on short-long exposure image pairs collected from specific camera models, and thus these approaches are less practical and generalizable in real-world settings where camera-specific joint enhancement and restoration is required. To tackle this problem, in this paper, we propose a low-light image processing framework that performs joint illumination adjustment, color enhancement, and denoising. Considering the difficulty in model-specific data collection and the ultra-high definition of the captured images, we design two branches: a coefficient estimation branch as well as a joint enhancement and denoising branch. The coefficient estimation branch works in a low-resolution space and predicts the coefficients for enhancement via bilateral learning, whereas the joint enhancement and denoising branch works in a full-resolution space and performs joint enhancement and denoising in a progressive manner. In contrast to existing methods, our framework does not need to recollect massive data when being adapted to another camera model, which significantly reduces the efforts required to fine-tune our approach for practical usage. Through extensive experiments, we demonstrate its great potential in real-world low-light imaging applications when compared with current state-of-the-art methods.

**Index Terms**—convolutional neural network, low-light image denoising, low-light image enhancement.

## I. INTRODUCTION

SMARTPHONE cameras dominate in terms of the global market share for all digital cameras. On top of them being highly compact and easy-to-use, the convenience of direct photo sharing through the internet means most people nowadays capture daily moments via phone cameras. In most cases where the surroundings are sufficiently bright, such as in sunny outdoor scenery, the images produced by these phone cameras have satisfactory quality in terms of brightness, noise level, and color aesthetic. Unfortunately, this cannot be guaranteed when it comes to low-light imaging: First, phone cameras are usually equipped with a relatively small aperture, which limits the amount of photons received by the sensor, resulting in low intensity for most pixels; Second, during the conversion from analog signals to digitized pixel values in image signal processing (ISP), various types of noise are introduced; Third, to avoid motion blur introduced by hand

shaking, exposure time should be within the safe shutter speed [1]. Consequently, the images obtained in low-light environments often have a low signal-to-noise ratio (SNR) with heavily underexposed regions and dull color, which not only fail to deliver sufficient information to the viewers but also affect the performance of computer vision applications such as face recognition [2].

To improve the quality of low-light images, some efforts have been made on hardware and software. While the former tries to improve the quantum efficiency of sensors or add artificial light sources such as infrared and ultraviolet flashes [3], the latter does not need extra costs and therefore is more popular. Some publicly available photo editors such as Lightroom provide a rich set of settings for users to manually alter photos according to their own preferences. Although the results can be of higher aesthetic quality, the editing process requires solid backgrounds that are not friendly for non-professionals. The significant time and efforts spent on manual adjustments also make it impractical for online social interactions. In addition to manual tools, there are several built-in photo enhancers in smartphones that can process images automatically. However, these are only suitable for minor alterations, and are thus less helpful for low-light enhancement where greater efforts are required.

Compared with general enhancements for well-lit images, quality improvement for images taken in low-light is more challenging. Non-learning-based studies [4]–[6] that mainly focused on handcrafted priors yielded limited performance in recovering details and color. A recent trend is to apply convolutional neural network (CNN) to learn a better non-linear mapping, which has shown a tremendous performance boost in enhancing both global and local contents. Nevertheless, there are still certain areas that can be improved: Most of the current methods are designed for only a single task, such as illumination enhancement or color enhancement, while the aesthetic quality is more than just a single aspect. Also, denoising is either missing, which is not aligned with the fact that sensor-specific noise universally appears in low-light images and may vary a lot between cameras, or heavily relies on paired training data for its removal, which is limited to the specific camera used for making the dataset and not directly applicable when being adapted to other cameras.

We claim that a good low-light image should have the following four characteristics: (a) sufficient illumination; (b) adequate contrast; (c) vivid color; and (d) low noise level. To meet these requirements, in this paper, we present a learning-based framework that performs joint enhancement and denoising for low-light images. We design a two-branch structure that

*Corresponding author: Seung-Won Jung.*

Y. Lu is with the Department of Multimedia Engineering, Dongguk University, Seoul, Korea. S.-W. Jung is with the Department of Electrical Engineering, Korea University, Seoul, Korea.

learns features for enhancement and denoising separately but applies them to the input image simultaneously. Particularly, the coefficient estimation branch operates in a low-resolution space that is noise-insensitive, and predicts parameters that can be used to enhance input images with arbitrary resolution. The joint enhancement and denoising branch operates in a full-resolution space, and performs camera-specific denoising along with enhancement in a progressive manner. To make full use of several existing datasets [7]–[9], we design a strategy that trains the coefficient estimation branch in a weakly supervised manner and the joint enhancement and denoising branch in an iterative manner. By using this approach, the proposed framework successfully learns a wide range of highly non-linear operations, resulting in high quality low-light images. Moreover, the design of the two-branch structure takes advantage of low computational complexity as well as easy applicability to other camera models without the need of recollecting a massive amount of training data. In summary, our contributions are three-fold:

- We present a framework that performs joint enhancement and denoising of low-light images. The proposed framework results in images with higher quality in comparison to current state-of-the-art methods both qualitatively and quantitatively.
- We design a two-branch structure that estimates enhancement parameters in low-resolution via bilateral learning, and applies joint enhancement and denoising in full-resolution in a progressive manner. This design enables the former to have a large receptive field that is insensitive to noise, while preserving high-resolution features for the latter.
- We propose a strategy that makes full use of several existing datasets developed for enhancement and denoising, respectively. For the coefficient estimation branch, a carefully designed loss function combined with zero-reference loss and color loss enables weakly supervised learning of the network. For the joint enhancement and denoising branch, a synthetic but realistic noise model is estimated for each camera model using only a few dark image samples, and then a synthetic paired dataset is generated and used for supervised learning of the network.

The rest of this paper is organized as follows: Section II reviews previous research related to our work; Section III describes the proposed framework and the details of each component; Section IV analyzes the proposed framework and presents the experiment results in comparison with state-of-the-art methods; and Section V concludes the paper and discusses our future work.

## II. RELATED WORKS

This section presents previous works related to the problems we address in this paper. We grouped them into three categories, namely image enhancement, image denoising, and joint enhancement and denoising.

### A. Image Enhancement

Images taken in low-light environments often contain poor visibility and dull color, where the former is the consequence of insufficient illumination and the latter is dependent on the illumination distribution of the captured scene. These images can be enhanced by extracting the illumination and reflectance components according to the Retinex theory [10]. Many methods have been proposed to recover these two components: Guo *et al.* [11] proposed an optimization framework to extract the illumination map and enhance it using gamma correction. Zhang *et al.* [12], [13] designed a series of handcrafted constraints and used relative total variation [14] to extract a structure-insensitive illumination map. Zhang *et al.* [15] generated a normal illumination map along with its inverted version and then fused them to obtain the final result.

Besides the Retinex theory-based methods, it is feasible for networks to learn a direct mapping with the help of paired data. Inspired by the bilateral guided upsampling [16], Gharbi *et al.* [17] proposed a light-weight network that learns a series of enhancement operations. This idea has been further extended and improved in [18] and [19]. Huang *et al.* [20] proposed a Laplacian enhancing unit to enhance image features from different scales, and combined the pixel-wise scaling and addition operations into final image reconstruction. In a similar way, Afifi *et al.* [21] built a coarse-to-fine exposure correction method using overexposed and underexposed image pairs. Ren *et al.* [22] proposed a hybrid network that handles global contents and local details separately. Similar work was presented in [23], where two-stage training was conducted with and without paired data. Moran *et al.* [24] applied a set of differentiable filters to the initial enhancement output from a U-Net-like network [25]. Wang *et al.* [26] proposed a network consisting of several lightening back-projection blocks that perform enhancement in an iterative manner.

The training of the above methods all requires a large amount of paired images, which are time-consuming and laborious to obtain. Therefore, learning from unpaired data has also attracted considerable attention. To achieve aesthetic-driven color enhancement, Deng *et al.* [27] employed a generative adversarial network (GAN) [28] to supervise the aesthetic quality of generated images. Chen *et al.* [29] proposed a two-way GAN with ideas borrowed from CycleGAN [30]. Similarly, Chai *et al.* [31] conducted a polynomial transform with their two-way GAN and proposed a method for fast color enhancement. Jiang *et al.* [32] employed a relativistic discriminator [33] in their dual discriminator design, yielding more natural images with enhanced details. Guo *et al.* [34] designed several handcrafted constraints and also proposed an iterative enhancer.

### B. Image Denoising

Compared with well-lit images, low-light images heavily suffer from noise. A straightforward yet powerful method of noise reduction is burst imaging, where a bunch of images are taken sequentially within a short period and then fused to produce a single clean image. Although several efforts [8], [35], [36] have been made to minimize motion blur artifacts

during multi-frame merging, the time and efforts spent on taking and merging these images still introduce a burden to more practical applications in which a single shot is preferred.

Owing to the convenience of capturing a single shot in daily usage, single image denoising has gained significant attention. While early works based on image priors [37]–[39] have shown limited performance for low-light images, recent studies on dense CNNs, such as grouped residual dense network [40], densely connected U-Net [41], and multi-scale residual dense network [42], have greatly improved the denoising quality and reached state-of-the-art performance, as reported in [43], [44].

To train a model that captures noise statistics more precisely, some methods revisited the influence of demosaicing and tried to combine it with denoising: Gharbi *et al.* [45] trained a network using the noise level as an extra input, leading to a significant improvement in both demosaicing and denoising. Kokkinos *et al.* [46] introduced a residual denoising network that performs these joint operations iteratively. Qian *et al.* [47] presented a multi-task model for joint demosaicing, denoising, and super-resolution, where a residual-in-residual dense block [48] was used to obtain the optimal performance. Liu *et al.* [49] further employed a density map as a self-guidance for the network to help focus more on high frequency patterns.

Meanwhile, several works have focused on noise modeling. Foi *et al.* [50] proposed a joint Poisson and Gaussian model that better describes the signal-dependent noise as well as the signal-independent noise of the captured raw data. Similarly, Hasinoff *et al.* [51] combined the two forms of noise in one single heteroscedastic Gaussian model. Several CNNs [52]–[55] trained with these synthetic but realistic noisy images have reported state-of-the-art performance. Recently, Wei *et al.* [56] decomposed noise into multiple sources based on an ISP pipeline and employed the Tukey lambda distribution to obtain a more precise noise model. Wang *et al.* [57] approximated the shot noise as a Gaussian distribution and merged it with the readout noise distribution, resulting in a new unique Gaussian noise model that is invariant to camera settings such as ISO. These enhanced noise models further improve the denoising performance of existing CNNs.

### C. Joint Image Enhancement and Denoising

Because aesthetic degradation is often accompanied with heavy noise in low-light images, the above methods that target a single task become less effective in practical usage. Although the cascaded application of enhancement and denoising is feasible [58]–[60], it is preferable to jointly perform these operations. To this end, Su *et al.* [61] proposed a two-step noise suppression model, in which a noise-aware histogram is first obtained to prevent noise amplification during contrast enhancement, and then a just noticeable difference (JND) model is used to further suppress noise. Similarly, Yu *et al.* [62] refined the JND map using Weber’s law, which resulted in improved performance. Ren *et al.* [63] performed Retinex theory-based sequential image decomposition to obtain a smooth illumination map as well as a noise-free reflectance map that allow for further adjustment. Li *et al.* [64] modified the Retinex model with a noise term and proposed an optimization method that predicts illumination, reflectance, and noise

map simultaneously. An improved version [65] is achieved with the help of a low-rank prior.

The joint task becomes more challenging when it comes to CNNs. Based on several datasets [59], [66] that provide short (noisy) and long (clean) exposure image pairs, a certain amount of progress has been made [67]–[72]. Several works have exploited an alternative approach where synthetic noisy images were used during the training stage. Wang *et al.* [73] synthesized Poisson-Gaussian noise using a simplified inverted ISP pipeline and then trained their progressive Retinex model. Chang *et al.* [74] investigated the distributions between short-exposed, long-exposed, and exposure-corrected images and proposed an improved data synthesis method for their long-short-exposure fusion network.

There have also some works dedicated to unpaired learning. In [75], a two-stage GAN-based network was proposed, where the Retinex theory-based enhancement is performed first, followed by a denoiser trained with the help of pseudo triples, similar work is presented in [76] based on self-supervision. Yang *et al.* [77] proposed a semi-supervised network that performs band decomposition with denoising on the input image, and then recomposes them to ensure the aesthetic quality is aligned with human visual perception. Anantrasirichai *et al.* [78] adapted the CycleGAN structure [30] for enhancing high-resolution inputs via contextual colorization and denoising, while Yang *et al.* [79] combined full-supervision, self-supervision, and adversarial learning into their training strategy.

Despite the great progress that the above works have achieved, the quality of the obtained images remains unsatisfactory. Besides, most of these approaches heavily rely on existing paired datasets that are limited to certain camera models. Therefore, lots of efforts are required to recollect a massive amount of data when adapting the prior works to new cameras. In comparison, our proposed framework successfully addresses these concerns. An elaborate two-branch structure enables the enhancement and denoising to operate in a joint manner. To leverage the lack of paired data for multi-task learning, we also propose a weakly-supervised strategy to make the training feasible.

## III. PROPOSED METHOD

This section provides details of the proposed framework. We first present the overall pipeline to offer the reader a brief understanding of the workflow. Then we introduce the design of each branch in detail.

### A. Framework Overview

An overview of the proposed framework is shown in Fig. 1. It mainly consists of two branches: the coefficient estimation branch and the joint enhancement and denoising branch. Given an unprocessed camera raw image as the input, we first convert it to sRGB color space and resize to  $256 \times 256$ . There are two reasons for using the downsampled version instead of the original one: First, the receptive field of the network cannot cover the input images with ultra-high resolution, and thus the global information learned by the network can be incomplete;

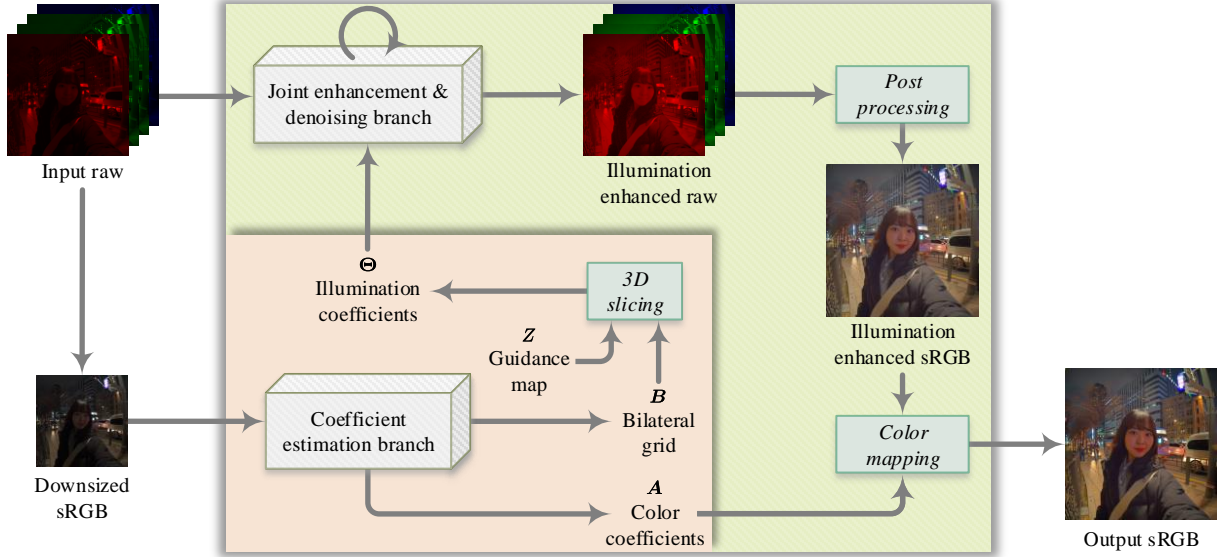


Fig. 1. Overview of the proposed two-branch framework. The coefficient estimation process is grouped in light pink, while the joint enhancement and denoising process is grouped in light olive.

Second, the effects of noise can be significantly suppressed by downsampling. The downsampled sRGB image is then passed to the coefficient estimation branch to learn two sets of adjustment parameters: the quadratic transform coefficients for illumination adjustment, and the polynomial transform coefficients for color adjustment. In contrast to the coefficient estimation branch, the joint enhancement and denoising branch processes the full-resolution raw image. In particular, an elaborate light-weight network performs joint illumination enhancement and denoising in a progressive manner, resulting in a denoised image with enhanced illumination. Next, after some post-processing operations, the enhanced raw image is demosaiced and converted to sRGB image, and a polynomial transformation is applied to enhance the color and contrast. As a result, the obtained image can achieve adequate illumination, good contrast, vivid color, and reduced noise.

The two-branch design takes advantage of several aspects in real-world mobile imaging. On one hand, the adjustment parameters are learned in low-resolution space, which gives not only the benefit of low consumption of hardware resources and fast processing speed, but also makes the process robust to different noise characteristics and arbitrary input resolutions. On the other hand, the enhancement and denoising are performed jointly, which is preferred as it allows avoiding the artifacts, such as amplified noise or over-smoothed details, which frequently occur in previous methods.

### B. Coefficient Estimation Branch

The main structure of the coefficient estimation branch is depicted in Fig. 2(a). The features of the downsampled sRGB image are extracted by an encoder at the early stage, here we employ MobileNet v2 [80] as the backbone feature extractor, in which all the batch-norm layers are removed. The sixth bottleneck module was empirically chosen as the output block because this module provides deeper features with stronger

encoding ability while keeping the spatial resolution of the output feature maps relatively high ( $16 \times 16$  for the input size of  $256 \times 256$ ). The extracted features are then shared for further prediction of the illumination enhancement and color enhancement coefficients.

For illumination enhancement, we observe that a human expert usually starts with global operations followed by local adjustments. Inspired by [17], we design two paths, namely global path and local path, to learn the features of global and local illumination adjustments, respectively. Since these adjustments do not work well when being applied separately (see Section IV-B for more details), we instead implicitly combine them in the feature space and use another convolution layer to map the fused features to the desired dimensions. The output is a set of bilateral grids, *i.e.*,  $\mathbf{B} = \{B_1, B_2, \dots, B_N\}$ , where  $N$  is the number of total iterations. Each  $B_n$  has the size of  $16 \times 16 \times 16$ . The full-resolution coefficient map  $\Theta_n$  is then obtained by the learned bilateral upsampling [17] via 3D slicing as follows:

$$\Theta_n(x, y) = \sum_{i,j,k} \tau(x, i) \tau(y, j) \tau(z_{x,y}, k) B_n(i, j, k), \quad (1)$$

where  $\tau$  is the linear interpolation kernel.  $(x, y)$  and  $(i, j, k)$  represent the pixel coordinates and the cell index of the bilateral grid, respectively.  $z_{x,y}$  is estimated from the pixel values at  $(x, y)$ , which will be explained in Section III-D. Note that all the coefficients for every iteration are obtained before the joint enhancement and denoising process.

In contrast to illumination adjustment, we notice that color retouching is often performed in a global manner. Therefore, we design a color path that extracts global features and predicts a set of polynomial coefficients  $A_K$  for the color enhancement, which will be explained later.

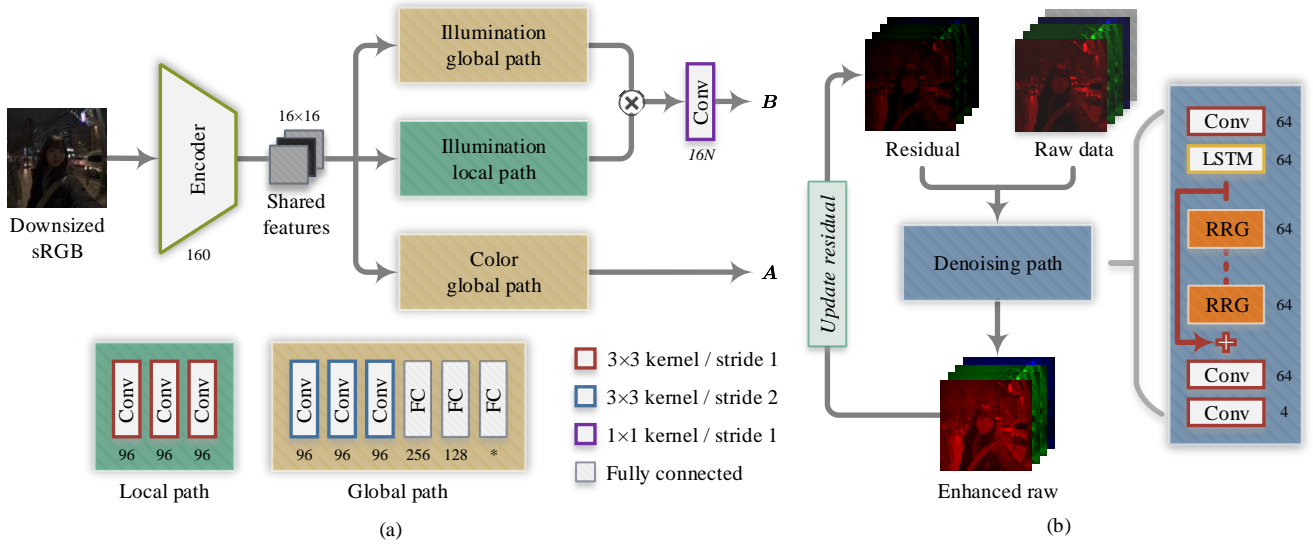


Fig. 2. Network structure of (a) the coefficient estimation branch and (b) the joint enhancement and denoising branch. Note that the raw data in (b) include the captured raw data  $I_0$  and its corresponding noise variance map  $V$ . The number of output channels is shown underneath or next to each layer.

### C. Progressive Enhancement without Denoising

For clarification purposes, we first explain how to perform progressive enhancement using  $\Theta_n$  and  $A_K$  without considering denoising. The image enhancement begins with progressive illumination adjustment that compensates for insufficient lighting in dark regions. Motivated by [34], the illumination adjustment at each iteration is performed through a quadratic transform function defined as follows:

$$I_n(\mathbf{x}) = I_{n-1}(\mathbf{x}) + \Theta_n(\mathbf{x})(1 - L_{n-1}(\mathbf{x}))I_{n-1}(\mathbf{x}), \quad (2)$$

where  $I_n$  and  $I_{n-1}$  are the images in camera raw color space from the current and the previous iterations, respectively.  $L_{n-1}$  is the luminance channel of  $I_{n-1}$  in XYZ color space.  $\mathbf{x}$  denotes a pixel coordinate vector, which will be omitted hereafter when unnecessary.

The image enhanced by the above step has improved illumination and details compared to the original input, but still lacks adequate contrast, saturation, and vivid color. Thus, color enhancement is applied to further improve the aesthetic quality. To this end, we adapt the polynomial transform [81]–[83] as the color enhancement operation, defined as follows:

$$J_O(\mathbf{x}) = \mathbf{A}_K \rho_K(J_N(\mathbf{x})), \quad (3)$$

where  $J_N$  represents the sRGB image converted from  $I_N$ , and  $J_O$  is the color-enhanced sRGB image.  $\rho_K(J_N(\mathbf{x}))$  is a column vector consisting of some polynomial terms of  $J_N(\mathbf{x})$  with the degree up to  $K$ , defined as follows:

$$\rho_K(J_N(\mathbf{x})) = [r^i g^j b^k \mid J_N(\mathbf{x}) = (r, g, b), i+j+k \leq K], \quad (4)$$

where  $i$ ,  $j$ , and  $k$  are non-negative integers. The effects of polynomial transform with different degrees will be discussed in Section IV-B.

### D. Joint Enhancement and Denoising Branch

Low-light images always come with obvious noise. More importantly, this noise can be amplified during the enhancement via (2)-(3). Therefore, we introduce a joint enhancement and denoising branch to tackle this issue.

Let  $R_n = \Theta_n(1 - L_{n-1})I_{n-1}$ , then (2) can be rewritten as follows:

$$\begin{aligned} I_N &= I_{N-1} + R_N \\ &= I_{N-2} + R_{N-1} + R_N \\ &= I_0 + R_1 + R_2 + \dots + R_{N-1} + R_N. \end{aligned} \quad (5)$$

apparently, the enhancement result  $I_N$  is the sum of the input  $I_0$  and all the residuals obtained from each iteration. Therefore, a residual network  $\mathcal{G}$  can be introduced to convert (5) to a single operation as follows:

$$I_N = \mathcal{G}\left(I_0, \sum_{n=1}^N R_n\right). \quad (6)$$

Although such network can be designed in a straightforward manner to perform (6), it does not work well for two reasons: First, the noise statistics are altered at each iteration, which makes the corresponding noise model hard to be estimated; Second, the sum of all the residuals contains accumulated noise, which further makes network training challenging. We consider this problem can be alleviated if the network can “memorize” the refined noise statistical features at each iteration. To this end, we insert a long short-term memory (LSTM) layer with a hidden state  $h$  into  $\mathcal{G}$  to have a recurrent residual network  $\mathcal{G}'$ . The update at the  $n$ -th iteration is therefore represented as follows:

$$\begin{cases} R_n = \Theta_n(1 - L_{n-1}^U)I_{n-1}^U, \\ \{I_n^U, h_n\} = \mathcal{G}'(I_0, V, R_n, h_{n-1}), \end{cases} \quad (7)$$

where  $I_n^U$  denotes the updated image.  $V$  is the pixel-wise noise variance obtained from camera metadata [84]. For the first iteration,  $I_0^U$  is obtained as follows:

$$\{I_0^U, h_0\} = \mathcal{G}'(I_0, V, \mathbf{0}, \mathbf{0}). \quad (8)$$

By using (7), the joint enhancement and denoising can be performed in a progressive manner. We adapt the iterative ResNet [85] and CycleISP [53] in the network design, the structure is shown in Fig. 2(b), where the recursive residual group (RRG) is composed of several densely-connected dual attention blocks (see Section IV-B for more details). From  $I_0^U$ , we also obtain the full-size guidance map  $Z$  that contains  $z_{x,y}$  values in (1) as follows:

$$Z = \mathcal{F}(I_0^U), \quad (9)$$

where  $\mathcal{F}$  is a mapping function learned by a simple network consisting of three convolutional layers.

Several other operations in the ISP pipeline such as demosaicing can also alter the noise statistics. Therefore, demosaicing, color space transformation are performed after the joint enhancement and denoising, resulting in an sRGB image  $J_N^U$ . Note that our goal is to learn perceptual quality enhancement rather than color correction, thus we assume the white point from camera metadata is correct and directly use it in calculating the camera color matrix [84]. Finally, by replacing  $J_N$  with  $J_N^U$  in (4), we obtain the final result with sufficient illumination, adequate contrast, vivid color, and reduced noise.

### E. Loss Function

In general, training a neural network requires massive paired data. However, to the best of our knowledge, there is no any dataset that contains low-light images of real-world scenes and their corresponding noise-free ground-truth images with expert enhanced illumination and color. In practice, making such a dataset is very challenging. Therefore, we design a strategy that trains the coefficient estimation branch in a weakly-supervised manner and the joint enhancement and denoising branch in a supervised manner using synthetic paired samples.

To train the coefficient estimation branch, we employ three loss terms, namely exposure loss, perceptual loss, and color loss. First, we adapt the weighting function from [86] as the exposure loss for encouraging the network to adjust both underexposed and overexposed regions to an adequate exposure range. The exposure loss is defined as follows:

$$\mathcal{L}_e = \frac{1}{M} \sum_{\mathbf{x}} \left( 1 - \exp \left( - \frac{(I_N(\mathbf{x}) - 0.5)^2}{2\delta^2} \right) \right), \quad (10)$$

where  $M$  is the total number of pixels, and  $\delta$  is a hyperparameter that controls the aesthetic quality.

Although the exposure loss is effective in enhancing illumination, it results in poor contrast if used alone. To preserve the overall perceptual quality, based on the observation that VGG models are not very sensitive to illumination changes [32], the Euclidean distance of VGG16 features is used as the

perceptual loss to ensure that the input and output images have similar feature representations:

$$\mathcal{L}_p = \frac{1}{5} \sum_{i=1}^5 \|\mathcal{V}_i(I_N) - \mathcal{V}_i(I_0)\|_2, \quad (11)$$

where  $\mathcal{V}_i$  represents the output features of the  $i$ -th block in the pre-trained VGG16 model [87].

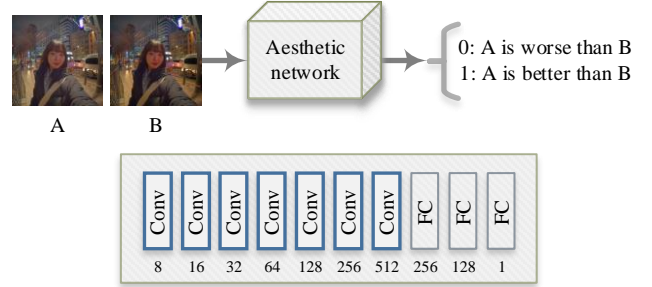


Fig. 3. Structure of the aesthetic network.

The color loss is more challenging because it is not easy to quantify the aesthetic quality of an image. Motivated by [88] that uses a pre-trained image assessment network as a part of the supervision, we employ an aesthetic network  $\mathcal{Q}$  that evaluates the aesthetic quality. However, we experienced difficulties in training the aesthetic network from only a single image, and we also noticed that the original untouched image can be used as a reference in the evaluation. Therefore, we adapt the relativistic classifier in [40] as the aesthetic network. As shown in Fig. 3, it uses paired images obtained before and after the color enhancement operation as ordered inputs, and predicts a binary label indicating whether the enhanced result has “better” (1) or “worse” (0) aesthetic quality. The color loss is defined as follows:

$$\mathcal{L}_c = \hat{y} (-\log(\mathcal{Q}(J_N, J_O))) + (1 - \hat{y}) (-\log(1 - \mathcal{Q}(J_O, J_N))), \quad (12)$$

where  $\hat{y}$  represents the ground-truth binary label. The final loss function for training the coefficient estimation branch is the combination of the three terms:

$$\mathcal{L}_E = \mathcal{L}_e + \mathcal{L}_p + \mathcal{L}_c. \quad (13)$$

Note that the aesthetic network is not trained with other branches. Instead, we train it separately using paired data and kept it fixed likewise with the pre-trained VGG16 model.

To train the joint enhancement and denoising branch, we freeze the coefficient estimation branch and compute the loss for each iteration as follows:

$$\mathcal{L}_D = \frac{1}{N+1} \sum_{n=0}^N \|I_n^U - I_n\|_1, \quad (14)$$

where  $I_n^U$  and  $I_n$  are obtained from (7) and (2) using noisy and clean raw images, respectively. As a result, the joint enhancement and denoising branch can learn how to denoise raw images during iterations.

### F. Noise Synthesis

The joint enhancement and denoising branch works on the camera raw domain whose noise statistics are device-dependent. Therefore, retraining of this branch is necessary for new camera models. To obtain sufficient data for retraining, a straightforward approach is to collect multiple images of the same scene with the same configuration for the given camera, and then fuse them to produce ground-truth images [89]. However, this approach is very time-consuming and sensitive to the misalignment of the captured images. A more convenient method is to synthesize realistic noisy-clean image pairs.

Specifically, our method requires one clean raw image dataset for all camera models, where we used the images from the RAISE dataset [9]. Given a new camera model, we estimate only the noise statistics and make noisy-clean pairs by adding the camera specific noise to clean raw images. Therefore, there is no need to recollect paired images for new camera models.

For the estimation of device-dependent noise statistics, we pay attention to two major sources of noise: photon noise from the quantum characteristics of photons and read noise from the readout circuitry. While the photon noise can be modeled as a Poisson random variable, the read noise has a much more complicated distribution. A commonly used model is to approximate it as a Gaussian random variable, which is computationally tractable but lacks accuracy. One recent work [56] investigated the physical characteristics of camera readout circuits and showed that the read noise can be better modeled as a mixture of readout noise  $N_r$ , horizontal banding noise  $N_h$ , and quantization noise  $N_q$ . Along with the photon noise  $N_p$ , their probability distributions are given as follows:

$$\begin{aligned} (E + N_p) &\sim \mathcal{P}(E), \\ N_r &\sim TL(\lambda_r; 0, \sigma_r), \\ N_h &\sim \mathcal{N}(0, \sigma_h), \\ N_q &\sim \mathcal{U}(-0.5s, 0.5s), \end{aligned} \quad (15)$$

where  $E$  is the number of photons and  $TL$  represents the Tukey lambda distribution with the shape determined by  $\lambda_r$ .  $\mathcal{P}$ ,  $\mathcal{N}$ , and  $\mathcal{U}$  represent the Poisson, Gaussian, and uniform distributions, respectively.  $s$  is the quantization step.

The parameters of the above distributions for each ISO level can be acquired from a few image samples captured under completely dark environments. Given such images, the standard deviation  $\sigma_h$  is estimated using the mean values of each row from the raw images. The shape parameter  $\lambda_r$  and the standard deviation  $\sigma_r$  are estimated using the probability plot correlation coefficient plot and probability plot (see [56] for more details), respectively. The final noise model  $N_f$  is defined as the combination of all the above noise sources:

$$N_f = \kappa N_p + N_r + N_h + N_q, \quad (16)$$

where  $\kappa$  is the photon transfer gain defined in the camera's calibration metadata. We thus estimate  $N_f$  for each camera model and generate synthetic paired noisy-clean images for training.

## IV. EXPERIMENT RESULTS

This section presents the experiment results and analysis. Particularly, each branch was first evaluated individually and then compared with its related state-of-the-arts. Then the whole framework was evaluated to fully reveal its promising potential. All our results reported are with color enhancement unless otherwise noticed.

### A. Implementation Details

For the coefficient estimation branch, we found that the bilateral slicing operation and the weakly-supervised loss function raise the difficulty in training from scratch. We thus performed pre-training to handle this issue, where we used the untouched sRGB images from the Adobe FiveK dataset [7] and generated linear and non-linear sRGB image pairs as training data. This pre-training process encourages the network to learn an initial mapping from linear sRGB to non-linear sRGB image, which was found to be very effective for the convergence of subsequent training. The ‘‘Expert C’’ subset of the same dataset was used to train the aesthetic network. Note that we modified the input images to match the exposure levels of the retouched images to avoid biased learning due to exposure differences. After that, we fixed the aesthetic network and trained only the coefficient estimation branch. For this fine-tuning, training images were chosen from the clean raw (obtained in burst mode) subset of the HDR+ dataset [8]. We used the same input resolution of  $256 \times 256$  in both the pre-training and the fine-tuning to avoid image resizing.

For the joint enhancement and denoising branch, we selected the ‘‘Outdoor’’ subset of the RAISE dataset [9] as the training set. To generate degraded images, the original raw images were first darkened by random scales in the range of 1-16 which simulates exposure compensation of up to 4 stops, and then cropped to  $64 \times 64$  and mixed with the synthetic noise.

The proposed framework was implemented in PyTorch and trained on an Nvidia Titan RTX GPU. The source code is available on our project website<sup>1</sup>.

### B. Component Analysis

The proposed framework performs three operations, namely illumination adjustment, color enhancement, and denoising. To find out the optimal configuration for these operations, we conducted three experiments.

First, we examined the performance of the illumination adjustment. To this end, we applied (2) with different numbers of iterations ranging from 2 to 16, and trained each variant on a modified version of the Adobe FiveK dataset without color shift. The results are depicted in Fig. 4. It can be seen that the average PSNR gradually increases for about 9 iterations and then starts to fluctuate. Based on this observation, we set  $N = 9$  as the default.

Next, we examined the performance of the color adjustment. To this end, we selected eight types of polynomial transforms with various degrees, and trained each variant on a modified

<sup>1</sup><https://github.com/YCL92/LowlightENR>

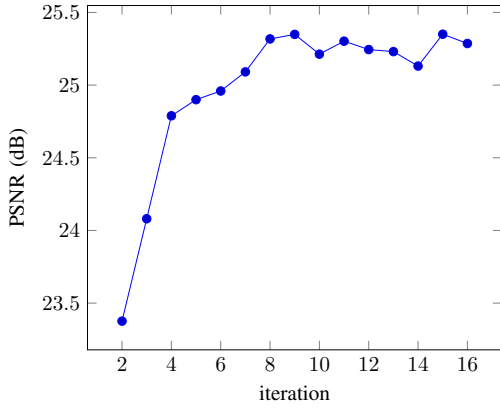


Fig. 4. Illumination adjustment results of different numbers of iterations.

version of the Adobe FiveK dataset without exposure shift. The first four candidates,  $\rho_1$ - $\rho_4$ , are expressed as follows:

$$\left\{ \begin{array}{l} \rho_1 = [r, g, b, 1]^T, \\ \rho_2 = [r^2, g^2, b^2, rg, gb, rb, r, g, b, 1]^T, \\ \rho_3 = [r^3, g^3, b^3, rg^2, gb^2, rb^2, gr^2, bg^2, br^2, r, g, b, 1]^T, \\ \rho_4 = [r^4, g^4, b^4, r^3g, r^3b, g^3r, g^3b, b^3r, b^3g, \\ r^2g^2, g^2b^2, r^2b^2, r^2gb, g^2rb, b^2rg, \\ r^3, g^3, b^3, rg^2, gb^2, rb^2, gr^2, bg^2, br^2, r, g, b, 1]^T. \end{array} \right. \quad (17)$$

 TABLE I  
 COLOR ADJUSTMENT RESULTS OF DIFFERENT POLYNOMIAL TRANSFORMS

Polynomial	$\bar{\rho}_1$	$\bar{\rho}_2$	$\bar{\rho}_3$	$\bar{\rho}_4$
PSNR	19.1429	24.6043	28.2288	28.3260
Polynomial	$\rho_1$	$\rho_2$	$\rho_3$	$\rho_4$
PSNR	26.6424	31.6538	33.7718	34.9111

The remaining four candidates,  $\bar{\rho}_1$ - $\bar{\rho}_4$ , are obtained by excluding the constant term “1” from  $\rho_1$ - $\rho_4$ , respectively. As shown in Table I,  $\rho_4$  resulted in the best performance but with significant computation cost, and we thus chose  $\rho_3$  as the default.

 TABLE II  
 DENOISING RESULTS OF DIFFERENT DENOISING NETWORK CONFIGURATIONS IN TERMS OF PSNR

$n_r/n_d$	2/3	3/2	2/4	4/2	2/5	5/2
PSNR	39.9417	39.9964	40.1302	40.0832	40.1827	40.4202
$n_r/n_d$	2/6	6/2	2/7	7/2	2/8	8/2
PSNR	40.2359	40.7132	40.3649	40.7388	40.5656	40.8680
$n_r/n_d$	3/3	3/4	4/3	3/5	5/3	4/4
PSNR	40.2093	40.4257	40.4020	40.3981	40.6784	40.6167

After that, we tested the performance of the joint enhancement and denoising branch. To this end, we trained a series

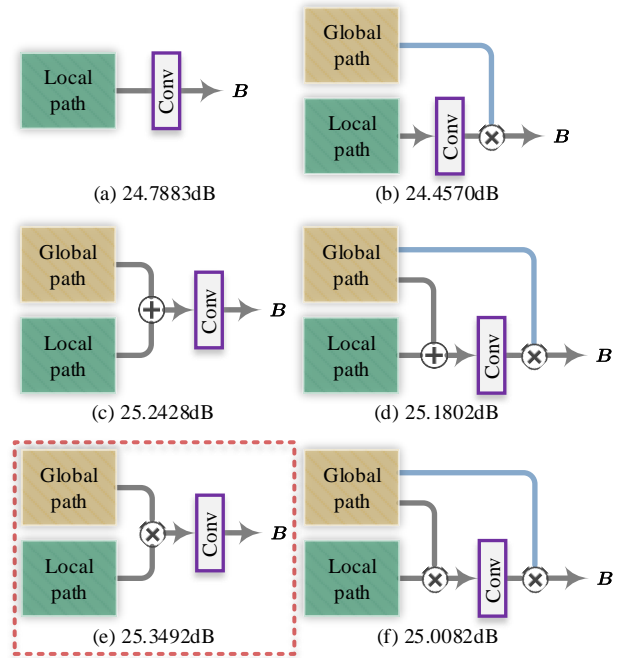
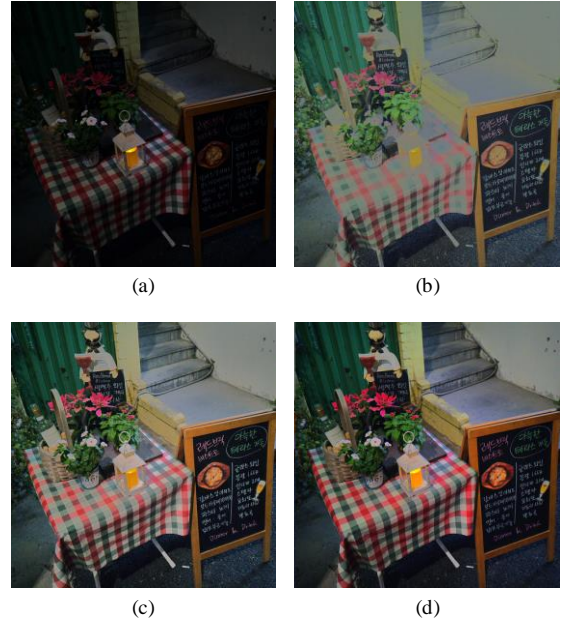


Fig. 5. Variants of the illumination coefficient estimation path and their corresponding average PSNRs on the Adobe FiveK validation dataset. Note that the blue line indicates per-iteration multiplication.


 Fig. 6. Enhancement results trained with different loss function variants: (a) without  $\mathcal{L}_e$ ; (b) without  $\mathcal{L}_p$ ; (c) without  $\mathcal{L}_c$ ; (d) with all  $\mathcal{L}_e$ ,  $\mathcal{L}_p$ , and  $\mathcal{L}_c$ .

of variants with different numbers of dual attention blocks (dubbed  $n_d$ ) and recursive residual groups (dubbed  $n_r$ ) using the SIDD dataset [89]. The enhancement coefficients were estimated from the clean images and kept fixed for all network variants. To reduce computation complexity, we limited the number of convolution layers so that  $n_r n_d \leq 16$ . From the results shown in Table II, we found that a deeper network indeed helps improve the performance at the expense of

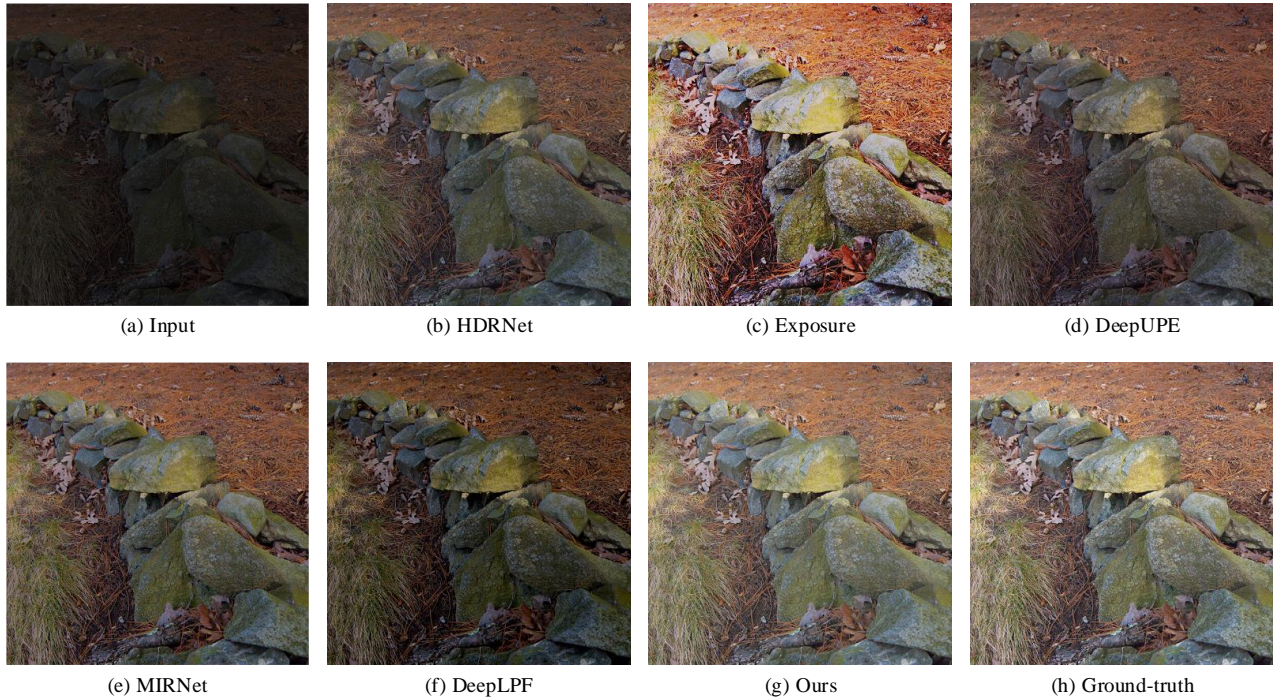


Fig. 7. An example of the visual comparison of ours and several state-of-the-art image enhancement methods on the Adobe FiveK dataset.

computation costs, and we set  $n_r = 6$  and  $n_d = 2$  considering the trade-off between accuracy and computational efficiency.

We then evaluated the individual components in each branch. For the joint enhancement and denoising branch, we found that removing the LSTM module leads to significant performance deterioration from 40.7132dB to 34.5686dB, which is aligned with our analysis in Section III-D. For the illumination coefficient estimation, several variants as shown in Fig. 5 were tested. It can be seen that embedding global operations implicitly in the feature space helps learn a better understanding of the overall context, which enables further improvement of the image quality. In comparison, separate adjustments outside the network do not deliver sufficient global information and thus degrade the performance.

In addition to the network structure, the loss function was also tested. Fig. 6 shows the results obtained by the networks trained with different loss function variants. Apparently, each component in the proposed loss function plays an essential role in network training.

### C. Evaluation of Coefficient Estimation Branch

To demonstrate the learning ability of the proposed coefficient estimation branch, we first trained it under full supervision using paired data for 300 epochs with L2 loss. For the performance comparison, five state-of-the-art image enhancement methods that use paired datasets for training were selected, namely HDRNet [17], Exposure [90], DeepUPE [19], MIRNet [70], and DeepLPF [24]. We retrained all the compared methods using their publicly available code and default parameter settings. The ‘‘Expert C’’ subset of the Adobe FiveK dataset was used for both training and testing. We followed the same dataset partition protocol described in [19].

After that, we applied all models to full-resolution test images (ranging from 1 to 16 megapixels) and computed PSNR and SSIM as the evaluation metrics. Fig. 7 shows an example of the visual comparison results. It can be seen that our method successfully improved the quality of the input image so that the resultant image looks more natural and close to the ground-truth. This can be further proved by the quantitative evaluation results listed in Table III. The proposed method outperforms all the other state-of-the-art methods, indicating that it can learn a more precise model of expert’s complicated retouching effects. In comparison, the encoder-decoder-based methods [24], [70] do not work well on these large input images, whereas the direct mapping-based methods [17], [19] show less effectiveness in learning more diverse enhancement operations.

TABLE III  
ENHANCEMENT RESULTS ON THE ADOBE FIVEK DATASET

Method	PSNR		SSIM	
	mean	std	mean	std
HDRNet [17]	23.3912	5.4072	0.9290	0.0568
Exposure [90]	18.4698	<b>3.6172</b>	0.7649	0.0971
DeepUPE [19]	23.3498	4.5180	0.9129	0.0555
MIRNet [70]	22.2512	4.3131	0.9028	0.0674
DeepLPF [24]	17.3689	3.9721	0.7576	0.1047
Ours	<b>25.8083</b>	5.2333	<b>0.9508</b>	<b>0.0530</b>

Another experiment was performed to evaluate the coefficient estimation branch under weak supervision. To this end, we selected six handcrafted or unpaired-learning-based image enhancement methods, namely LIME [11], JED [63], LR3M [65], AutoExp [15], Enlighten [32], and ZeroDCE [34], and

directly applied them to the full-size short exposure set of the SID dataset [66] which was unseen during the training. From Fig. 8, it can be clearly seen that our method successfully recovered the details and also improved the aesthetic quality. On the other hand, the other methods failed to produce images with high aesthetic quality, and some even generated unfavorable artifacts that heavily degrade the image. For the quantitative performance comparison, since the SID dataset contains long exposure images, we used them as the ground-truth in measuring the full-reference metrics, *i.e.*, PSNR and SSIM. We also employed several no-reference metrics, *i.e.*, information entropy (IE), global contrast factor (GCF) [91], and no-reference image quality metric for contrast distortion (NIQMC) [92], to evaluate the perceptual image quality. As shown in Table IV, our method shows better performance than the others by a significant margin, indicating that the coefficient estimation branch trained with unpaired data can be well generalized to unseen images. Note that the short-long exposure image pairs in the SID dataset were captured using the same camera configuration except exposure time. Therefore, any operation that alters color distribution results in lower PSNR and SSIM.

#### D. Evaluation of Joint Enhancement and Denoising Branch

The joint enhancement and denoising avoids breaking the noise statistics or over-smoothing the input image in comparison with a cascaded application of denoising and enhancement. For the performance comparison, we tested two representative methods of handcrafted and learning-based raw denoising, namely BM3D [93] and CycleISP [53]. In particular, we examined two scenarios: denoising followed by enhancement (dubbed den-enh) and enhancement followed by denoising

TABLE IV  
ENHANCEMENT RESULTS ON THE SID DATASET

Method	PSNR	SSIM	IE	GCF	NIQMC
LIME [11]	16.8685	0.4630	6.2399	4.1678	3.6991
JED [34]	13.0279	0.3370	3.9429	0.7070	1.0918
LR3M [65]	12.3882	0.2578	3.8935	0.6433	0.8926
AutoExp [15]	14.4591	0.3798	5.5633	2.5777	2.8736
Enlighten [32]	14.8203	0.4503	4.9853	1.9282	2.4124
ZeroDCE [34]	12.6766	0.2243	4.6076	1.3056	1.8566
Ours (w/o CE*)	<b>18.2517</b>	<b>0.5098</b>	6.5087	4.6893	4.1004
Ours	18.0275	0.4998	<b>6.6182</b>	<b>4.9421</b>	<b>4.2210</b>

\* CE: color enhancement

(dubbed enh-den). We obtained a low-light subset of the SIDD dataset, where we collected samples with the attribute of “Lowlight” from SIDD-Small as the test set, and split the rest samples from SIDD-Full into a ratio of 95:5 for training and validation, respectively. The enhancement results without denoising were used as the baseline. All networks were retrained using their default settings for a fair comparison.

TABLE V  
DENOISING RESULTS ON THE SIDD DATASET

Method	Order	PSNR		SSIM	
		mean	std	mean	std
Baseline	N/A	24.6193	5.1711	0.5684	0.2307
BM3D [93]	den-enh	33.1984	4.8243	0.8926	0.0959
	enh-den	24.7132	5.2054	0.5724	0.2310
CycleISP [53]	den-enh	37.0623	<b>3.9643</b>	0.9572	0.0450
	enh-den	36.7755	4.7570	0.9477	0.0630
Ours	joint	<b>39.7626</b>	4.0641	<b>0.9731</b>	<b>0.0316</b>



Fig. 8. An example of the visual comparison of ours and several state-of-the-art image enhancement methods on the SID dataset.

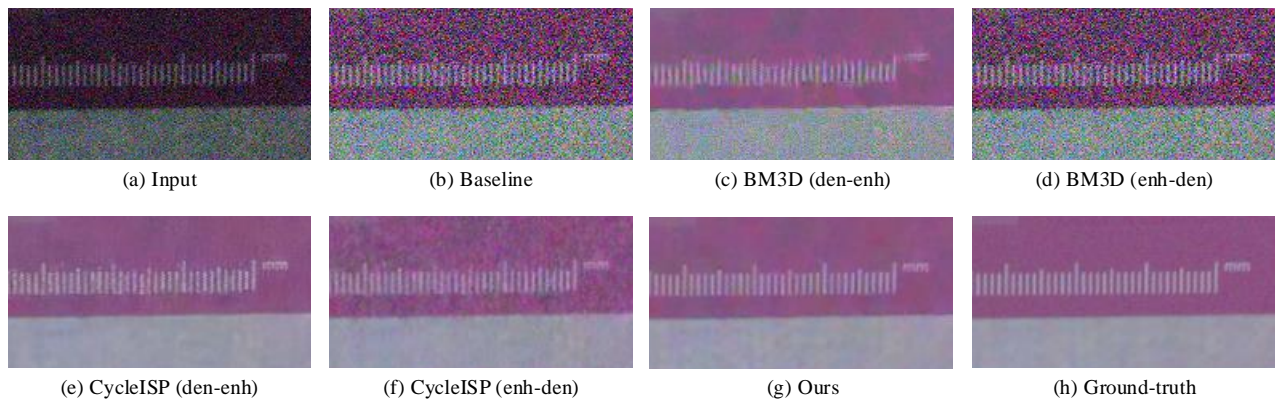


Fig. 9. An example of the visual comparison of ours and several state-of-the-art image denoising methods on the SIDD dataset.

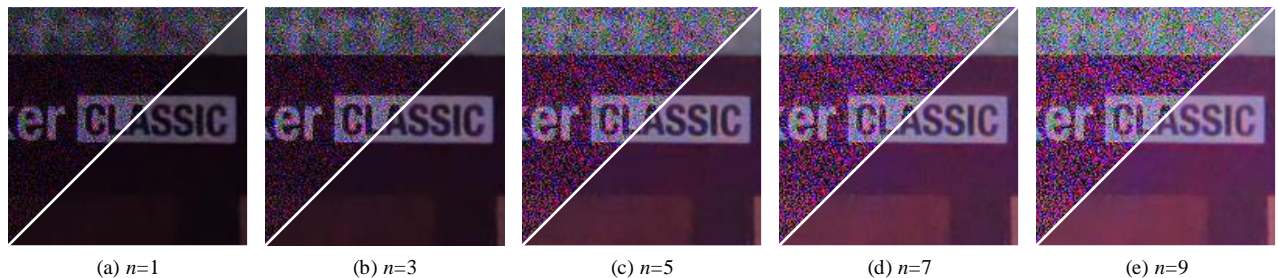


Fig. 10. An example of the intermediate enhancement results obtained after  $n$  iterations with and without denoising on the SIDD dataset.

Fig. 9 shows the resultant image examples. It can be seen that cascaded networks either failed in denoising or over-smoothed the image details. Compared to the others, our joint enhancement and denoising successfully preserved the details and suppressed the noise. This can also be observed from the intermediate results shown in Fig. 10, where the noise was heavily amplified during the progressive enhancement without denoising as explained in Section III-C. Table V lists the quantitative results, which show evident performance drop in cascaded architectures regardless of processing order. In comparison, our joint method outperforms all the others by a significant margin.

### E. Evaluation of Combined Framework

In order to evaluate the complete framework, we made a small dataset obtained from four mobile devices, *i.e.*, DJI Osmo Action, Google Pixel 3, Apple iPhone 11, and Samsung Galaxy S20. Each device was used to capture 20 raw low-light images with various types of objects including selfies,

buildings, and streets. We used the safe shutter speed to avoid motion blur and limited the ISO below 400 to preserve highlights. In this experiment, the neural image assessment (NIMA) [94], which is of high correlation to human perception and capable of no-reference image quality assessment in terms of illumination, color, noise level, and high-level aesthetic and semantic features, was used as the evaluation metric. We reported the performance of the proposed framework with eight state-of-the-art learning-based methods, namely Exposure [90], DeepUPE [19], MIRNet [70], DeepLPF [24], KinD [67], RetinexNet [59], EnlightenGAN [32], and ZeroDCE [34]. Each camera model was evaluated individually.

The evaluation results are summarized in Table VI. Our method received the highest NIMA scores among all the compared methods and produced consistent performance across four test devices, while the other methods showed lower performance and were unstable in cross-model enhancement. This can also be observed in Fig. 11: Most of the other methods either failed in recovering sufficient details in the

TABLE VI  
JOINT ENHANCEMENT AND DENOISING RESULTS IN TERMS OF NIMA SCORES ON OUR DATASET

Device	Exposure [90]	DeepUPE [19]	MIRNet [70]	DeepLPF [24]	KinD [67]	RetinexNet [59]	Enlighten [32]	ZeroDCE [34]	Ours
DJI	5.6085	5.6350	5.5286	5.7064	5.7027	4.6945	5.8717	5.3973	<b>5.9566</b>
iPhone11	4.7139	4.8477	4.7878	4.8585	4.7938	4.8192	4.8157	4.7659	<b>5.2594</b>
Pixel3	4.8353	4.9247	5.0571	4.9895	4.9639	4.6956	4.9985	4.7611	<b>5.3154</b>
S20	4.8871	4.9743	5.0065	5.0729	5.0294	4.6520	5.1566	4.7685	<b>5.3227</b>
mean	5.0112	5.0954	5.0950	5.1568	5.1224	4.7153	5.2106	4.9232	<b>5.4635</b>



Fig. 11. An example of the visual comparison of ours and several state-of-the-art image enhancement methods on our dataset.

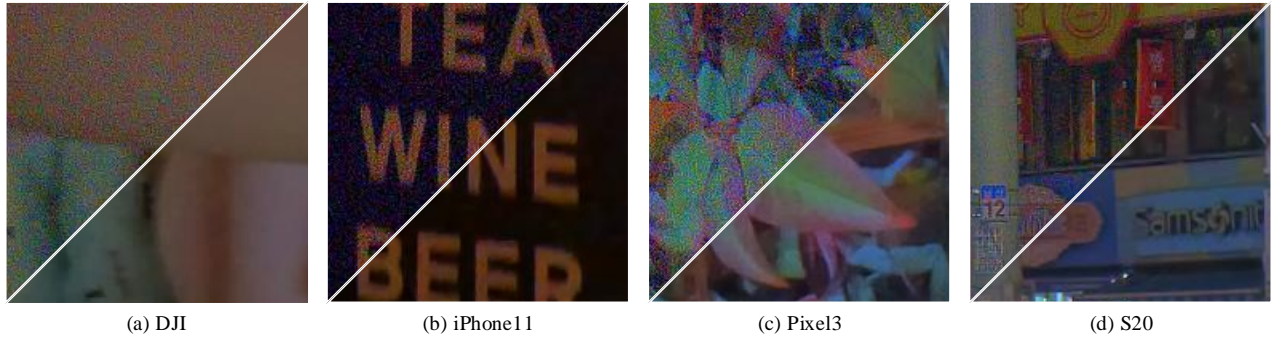


Fig. 12. Examples of enhancement results with and without denoising on four camera models.

dark regions (*e.g.*, the facial details in Figs. 11(b) and 11(e)) or over-enhanced bright regions (*e.g.*, the glowing ball in Figs. 11(d) and 11(e)). Some even resulted in undesired artifacts (*e.g.*, the background in Figs. 11(f) and 11(h)). By contrast, our method successfully recovered sufficient details in the dark areas while preserving the highlights and adjusted the overall color and contrast to further improve the aesthetic quality.

Another example of our joint enhancement and denoising is shown in Fig. 12. The two-branch design significantly relaxes the effort needed in cross-model noise reduction, resulting in clean images for all the test cameras used. In comparison, direct enhancement does not consider noise reduction and thus significantly amplifies noise, resulting in heavily degraded images that are more challenging for further improvement.

Last, we measured the computation complexity of the proposed method. The average processing time for our dataset (80 images with a resolution of approximately  $3,000 \times 3,000$ ) is 6.1687s, which is relatively fast considering our unoptimized code and models. We believe the efficiency can be further improved through optimization techniques such as post-training quantization [95].

## V. CONCLUSION

In this paper, we presented a learning-based framework for low-light image enhancement. In contrast to existing works, the proposed framework performs joint illumination enhancement, color enhancement, and model-specific denoising in a progressive manner. To make this approach practical in real-world applications, we designed a two-branch structure that handles coefficient estimation and joint enhancement and denoising in different domains. This design enables it to be retrained for a new camera model using only a few new image samples, which significantly reduces the human efforts required for recollecting massive amounts of paired data. Moreover, the joint process allows the network to be more robust and light-weight without compromising performance. Through extensive experiments, we showed that our framework outperforms existing state-of-the-art methods and successfully improves the quality of low-light images. Our future research directions include low-light white-balancing with semantic attention, universal model-independent raw denoising, multi-shot-based low-light imaging, and joint low-light image enhancement, denoising, and deblurring.

## REFERENCES

- [1] L. Yuan, J. Sun, L. Quan, and H.-Y. Shum, "Image deblurring with blurred/noisy image pairs," *ACM Trans. Graph.*, vol. 26, pp. 1–es, 2007.
- [2] J. Liu, D. Xu, W. Yang, M. Fan, and H. Huang, "Benchmarking low-light image enhancement and beyond," *Int. J. Comput. Vis.*, pp. 1–32, 2021.
- [3] D. Krishnan and R. Fergus, "Dark flash photography," *ACM Trans. Graph.*, vol. 28, 2009.
- [4] L. Yuan and J. Sun, "Automatic exposure correction of consumer photographs," in *Proceedings of ECCV*, 2012, pp. 771–785.
- [5] S. Wang, J. Zheng, H.-M. Hu, and B. Li, "Naturalness preserved enhancement algorithm for non-uniform illumination images," *IEEE Trans. Image Process.*, vol. 22, no. 9, pp. 3538–3548, 2013.
- [6] Q. Wang, X. Fu, X.-P. Zhang, and X. Ding, "A fusion-based method for single backlit image enhancement," in *Proceedings of ICIP*, 2016, pp. 4077–4081.
- [7] V. Bychkovsky, S. Paris, E. Chan, and F. Durand, "Learning photographic global tonal adjustment with a database of input/output image pairs," in *Proceedings of CVPR*, 2011, pp. 97–104.
- [8] S. W. Hasinoff, D. Sharlet, R. Geiss, A. Adams, J. T. Barron, F. Kainz, J. Chen, and M. Levoy, "Burst photography for high dynamic range and low-light imaging on mobile cameras," *ACM Trans. Graph.*, vol. 35, no. 6, pp. 1–12, 2016.
- [9] D.-T. Dang-Nguyen, C. Pasquini, V. Conotter, and G. Boato, "RAISE: A raw images dataset for digital image forensics," in *Proceedings of ACM MMSys*, 2015, pp. 219–224.
- [10] E. H. Land, "The retinex theory of color vision," *Scientific American*, vol. 237, no. 6, pp. 108–129, 1977.
- [11] X. Guo, Y. Li, and H. Ling, "LIME: Low-light image enhancement via illumination map estimation," *IEEE Trans. Image Process.*, vol. 26, no. 2, pp. 982–993, 2016.
- [12] Q. Zhang, G. Yuan, C. Xiao, L. Zhu, and W.-S. Zheng, "High-quality exposure correction of underexposed photos," in *Proceedings of ACM MM*, 2018, pp. 582–590.
- [13] Q. Zhang, Y. Nie, L. Zhu, C. Xiao, and W.-S. Zheng, "Enhancing underexposed photos using perceptually bidirectional similarity," *IEEE Trans. Multimedia*, 2020.
- [14] L. Xu, Q. Yan, Y. Xia, and J. Jia, "Structure extraction from texture via relative total variation," *ACM Trans. Graph.*, vol. 31, no. 6, pp. 1–10, 2012.
- [15] Q. Zhang, Y. Nie, and W.-S. Zheng, "Dual illumination estimation for robust exposure correction," *Comput. Graph. Forum*, vol. 38, no. 7, pp. 243–252, 2019.
- [16] J. Chen, A. Adams, N. Wadhwa, and S. W. Hasinoff, "Bilateral guided upsampling," *ACM Trans. Graph.*, vol. 35, no. 6, pp. 1–8, 2016.
- [17] M. Gharbi, J. Chen, J. T. Barron, S. W. Hasinoff, and F. Durand, "Deep bilateral learning for real-time image enhancement," *ACM Trans. Graph.*, vol. 36, no. 4, pp. 1–12, 2017.
- [18] K. Kong, J. Lee, W.-J. Song, M. Kang, K. J. Kwon, and S. G. Kim, "Multitask bilateral learning for real-time image enhancement," *J. Soc. Inf. Disp.*, vol. 27, no. 10, pp. 630–645, 2019.
- [19] R. Wang, Q. Zhang, C.-W. Fu, X. Shen, W.-S. Zheng, and J. Jia, "Underexposed photo enhancement using deep illumination estimation," in *Proceedings of CVPR*, 2019, pp. 6849–6857.
- [20] J. Huang, Z. Xiong, X. Fu, D. Liu, and Z.-J. Zha, "Hybrid image enhancement with progressive Laplacian enhancing unit," in *Proceedings of ACM MM*, 2019, pp. 1614–1622.
- [21] M. Afifi, K. G. Derpanis, B. Ommer, and M. S. Brown, "Learning to correct overexposed and underexposed photos," *arXiv preprint arXiv:2003.11596*, 2020.
- [22] W. Ren, S. Liu, L. Ma, Q. Xu, X. Xu, X. Cao, J. Du, and M.-H. Yang, "Low-light image enhancement via a deep hybrid network," *IEEE Trans. Image Process.*, vol. 28, no. 9, pp. 4364–4375, 2019.
- [23] H.-U. Kim, Y. J. Koh, and C.-S. Kim, "Global and local enhancement networks for paired and unpaired image enhancement," in *Proceedings of ECCV*, 2020.
- [24] S. Moran, P. Marza, S. McDonagh, S. Parisot, and G. Slabaugh, "DeepLPPF: Deep local parametric filters for image enhancement," in *Proceedings of CVPR*, 2020, pp. 12 826–12 835.
- [25] O. Ronneberger, P. Fischer, and T. Brox, "U-Net: Convolutional networks for biomedical image segmentation," in *Proceedings of MICCAI*, 2015, pp. 234–241.
- [26] L.-W. Wang, Z.-S. Liu, W.-C. Siu, and D. P. Lun, "Lightening network for low-light image enhancement," *IEEE Trans. Image Process.*, vol. 29, pp. 7984–7996, 2020.
- [27] Y. Deng, C. C. Loy, and X. Tang, "Aesthetic-driven image enhancement by adversarial learning," in *Proceedings of ACM MM*, 2018, pp. 870–878.
- [28] I. Goodfellow, J. Pouget-Abadie, M. Mirza, B. Xu, D. Warde-Farley, S. Ozair, A. Courville, and Y. Bengio, "Generative adversarial nets," in *Proceedings of NIPS*, 2014, pp. 2672–2680.
- [29] Y.-S. Chen, Y.-C. Wang, M.-H. Kao, and Y.-Y. Chuang, "Deep photo enhancer: Unpaired learning for image enhancement from photographs with GANs," in *Proceedings of CVPR*, 2018, pp. 6306–6314.
- [30] J.-Y. Zhu, T. Park, P. Isola, and A. A. Efros, "Unpaired image-to-image translation using cycle-consistent adversarial networks," in *Proceedings of ICCV*, 2017, pp. 2223–2232.
- [31] Y. Chai, R. Giryes, and L. Wolf, "Supervised and unsupervised learning of parameterized color enhancement," in *Proceedings of WACV*, 2020, pp. 992–1000.
- [32] Y. Jiang, X. Gong, D. Liu, Y. Cheng, C. Fang, X. Shen, J. Yang, P. Zhou, and Z. Wang, "EnlightenGAN: Deep light enhancement without paired supervision," *arXiv preprint arXiv:1906.06972*, 2019.
- [33] A. Jolicœur-Martineau, "The relativistic discriminator: A key element missing from standard GAN," *arXiv preprint arXiv:1807.00734*, 2018.
- [34] C. Guo, C. Li, J. Guo, C. C. Loy, J. Hou, S. Kwong, and R. Cong, "Zero-reference deep curve estimation for low-light image enhancement," in *Proceedings of CVPR*, 2020, pp. 1780–1789.
- [35] C. Godard, K. Matzen, and M. Uyttendaele, "Deep burst denoising," in *Proceedings of ECCV*, 2018, pp. 538–554.
- [36] O. Liba, K. Murthy, Y.-T. Tsai, T. Brooks, T. Xue, N. Karnad, Q. He, J. T. Barron, D. Sharlet, R. Geiss *et al.*, "Handheld mobile photography in very low light," *ACM Trans. Graph.*, vol. 38, no. 6, pp. 1–16, 2019.
- [37] A. Buades, B. Coll, and J.-M. Morel, "A non-local algorithm for image denoising," in *Proceedings of CVPR*, vol. 2, 2005, pp. 60–65.
- [38] M. Elad and M. Aharon, "Image denoising via sparse and redundant representations over learned dictionaries," *IEEE Trans. Image Process.*, vol. 15, no. 12, pp. 3736–3745, 2006.
- [39] S. Gu, L. Zhang, W. Zuo, and X. Feng, "Weighted nuclear norm minimization with application to image denoising," in *Proceedings of CVPR*, 2014, pp. 2862–2869.
- [40] D.-W. Kim, J. Ryun Chung, and S.-W. Jung, "GRDN: Grouped residual dense network for real image denoising and GAN-based real-world noise modeling," in *Proceedings of CVPR Workshops*, 2019, pp. 2086–2094.
- [41] B. Park, S. Yu, and J. Jeong, "Densely connected hierarchical network for image denoising," in *Proceedings of CVPR Workshops*, 2019, pp. 2104–2113.
- [42] L. Bao, Z. Yang, S. Wang, D. Bai, and J. Lee, "Real image denoising based on multi-scale residual dense block and cascaded U-Net with block-connection," in *Proceedings of CVPR Workshops*, 2020, pp. 448–449.
- [43] A. Abdelhamed, R. Timofte, and M. S. Brown, "NTIRE 2019 challenge on real image denoising: Methods and results," in *Proceedings of CVPR Workshops*, 2019, pp. 2197–2210.
- [44] A. Abdelhamed, M. Afifi, R. Timofte, and M. S. Brown, "NTIRE 2020 challenge on real image denoising: Dataset, methods and results," in *Proceedings of CVPR Workshops*, 2020, pp. 496–497.
- [45] M. Gharbi, G. Chaurasia, S. Paris, and F. Durand, "Deep joint demosaicking and denoising," *ACM Trans. Graph.*, vol. 35, no. 6, pp. 1–12, 2016.
- [46] F. Kokkinos and S. Lefkimmiatis, "Deep image demosaicking using a cascade of convolutional residual denoising networks," in *Proceedings of ECCV*, 2018, pp. 303–319.
- [47] G. Qian, J. Gu, J. S. Ren, C. Dong, F. Zhao, and J. Lin, "Trinity of pixel enhancement: A joint solution for demosaicking, denoising and super-resolution," *arXiv preprint arXiv:1905.02538*, 2019.
- [48] Y. Zhang, Y. Tian, Y. Kong, B. Zhong, and Y. Fu, "Residual dense network for image super-resolution," in *Proceedings of CVPR*, 2018, pp. 2472–2481.
- [49] L. Liu, X. Jia, J. Liu, and Q. Tian, "Joint demosaicking and denoising with self guidance," in *Proceedings of CVPR*, 2020, pp. 2240–2249.
- [50] A. Foi, M. Trimeche, V. Katkovnik, and K. Egiazarian, "Practical Poissonian-Gaussian noise modeling and fitting for single-image raw-data," *IEEE Trans. Image Process.*, vol. 17, no. 10, pp. 1737–1754, 2008.
- [51] S. W. Hasinoff, F. Durand, and W. T. Freeman, "Noise-optimal capture for high dynamic range photography," in *Proceedings of CVPR*, 2010, pp. 553–560.
- [52] T. Brooks, B. Mildenhall, T. Xue, J. Chen, D. Sharlet, and J. T. Barron, "Unprocessing images for learned raw denoising," in *Proceedings of CVPR*, 2019, pp. 11 036–11 045.

- [53] S. W. Zamir, A. Arora, S. Khan, M. Hayat, F. S. Khan, M.-H. Yang, and L. Shao, "CycleISP: Real image restoration via improved data synthesis," in *Proceedings of CVPR*, 2020, pp. 2696–2705.
- [54] I. Marras, G. G. Chrysos, I. Alexiou, G. Slabaugh, and S. Zafeiriou, "Reconstructing the noise manifold for image denoising," *arXiv preprint arXiv:2002.04147*, 2020.
- [55] H. Guan, L. Liu, S. Moran, F. Song, and G. Slabaugh, "NODE: Extreme low light raw image denoising using a noise decomposition network," *arXiv preprint arXiv:1909.05249*, 2019.
- [56] K. Wei, Y. Fu, J. Yang, and H. Huang, "A physics-based noise formation model for extreme low-light raw denoising," in *Proceedings of CVPR*, 2020, pp. 2758–2767.
- [57] Y. Wang, H. Huang, Q. Xu, J. Liu, Y. Liu, and J. Wang, "Practical deep raw image denoising on mobile devices," in *Proceedings of ECCV*, 2020.
- [58] L. Li, R. Wang, W. Wang, and W. Gao, "A low-light image enhancement method for both denoising and contrast enlarging," in *Proceedings of ICIP*, 2015, pp. 3730–3734.
- [59] C. Wei, W. Wang, W. Yang, and J. Liu, "Deep retinex decomposition for low-light enhancement," in *Proceedings of BMVC*, 2018.
- [60] Y. Guo, X. Ke, J. Ma, and J. Zhang, "A pipeline neural network for low-light image enhancement," *IEEE Access*, vol. 7, pp. 13 737–13 744, 2019.
- [61] H. Su and C. Jung, "Low light image enhancement based on two-step noise suppression," in *Proceedings of ICASSP*, 2017, pp. 1977–1981.
- [62] L. Yu, H. Su, and C. Jung, "Joint enhancement and denoising of low light images via jnd transform," in *Proceedings of ICASSP*, 2020, pp. 2658–2662.
- [63] X. Ren, M. Li, W.-H. Cheng, and J. Liu, "Joint enhancement and denoising method via sequential decomposition," in *Proceedings of ISCAS*, 2018, pp. 1–5.
- [64] M. Li, J. Liu, W. Yang, X. Sun, and Z. Guo, "Structure-revealing low-light image enhancement via robust retinex model," *IEEE Trans. Image Process.*, vol. 27, no. 6, pp. 2828–2841, 2018.
- [65] X. Ren, W. Yang, W.-H. Cheng, and J. Liu, "LR3M: Robust low-light enhancement via low-rank regularized retinex model," *IEEE Trans. Image Process.*, vol. 29, pp. 5862–5876, 2020.
- [66] C. Chen, Q. Chen, J. Xu, and V. Koltun, "Learning to see in the dark," in *Proceedings of CVPR*, 2018, pp. 3291–3300.
- [67] Y. Zhang, J. Zhang, and X. Guo, "Kindling the darkness: A practical low-light image enhancer," in *Proceedings of ACM MM*, 2019, pp. 1632–1640.
- [68] J. Zhang, R. Liu, L. Ma, W. Zhong, X. Fan, and Z. Luo, "Principle-inspired multi-scale aggregation network for extremely low-light image enhancement," in *Proceedings of ICASSP*, 2020, pp. 2638–2642.
- [69] C. Zhang, Q. Yan, Y. Zhu, X. Li, J. Sun, and Y. Zhang, "Attention-based network for low-light image enhancement," in *Proceedings of ICME*, 2020, pp. 1–6.
- [70] S. W. Zamir, A. Arora, S. Khan, M. Hayat, F. S. Khan, M.-H. Yang, and L. Shao, "Learning enriched features for real image restoration and enhancement," *arXiv preprint arXiv:2003.06792*, 2020.
- [71] Y. Atoum, M. Ye, L. Ren, Y. Tai, and X. Liu, "Color-wise attention network for low-light image enhancement," in *Proceedings of CVPR Workshops*, 2020, pp. 506–507.
- [72] K. Xu, X. Yang, B. Yin, and R. W. Lau, "Learning to restore low-light images via decomposition-and-enhancement," in *Proceedings of CVPR*, 2020, pp. 2281–2290.
- [73] Y. Wang, Y. Cao, Z.-J. Zha, J. Zhang, Z. Xiong, W. Zhang, and F. Wu, "Progressive retinex: Mutually reinforced illumination-noise perception network for low-light image enhancement," in *Proceedings of ACM MM*, 2019, pp. 2015–2023.
- [74] M. Chang, H. Feng, Z. Xu, and Q. Li, "Low-light image restoration with short-and long-exposure raw pairs," *arXiv preprint arXiv:2007.00199*, 2020.
- [75] W. Xiong, D. Liu, X. Shen, C. Fang, and J. Luo, "Unsupervised real-world low-light image enhancement with decoupled networks," *arXiv preprint arXiv:2005.02818*, 2020.
- [76] Y. Zhang, X. Di, B. Zhang, Q. Li, S. Yan, and C. Wang, "Self-supervised low light image enhancement and denoising," *arXiv preprint arXiv:2103.00832*, 2021.
- [77] W. Yang, S. Wang, Y. Fang, Y. Wang, and J. Liu, "From fidelity to perceptual quality: A semi-supervised approach for low-light image enhancement," in *Proceedings of CVPR*, 2020, pp. 3063–3072.
- [78] N. Anantrasirichai and D. Bull, "Contextual colorization and denoising for low-light ultra high resolution sequences," *arXiv preprint arXiv:2101.01597*, 2021.
- [79] Q. Yang, Y. Wu, D. Cao, M. Luo, and T. Wei, "A lowlight image enhancement method learning from both paired and unpaired data by adversarial training," *Neurocomputing*, vol. 433, pp. 83–95, 2021.
- [80] M. Sandler, A. Howard, M. Zhu, A. Zhmoginov, and L.-C. Chen, "MobileNetV2: Inverted residuals and linear bottlenecks," in *Proceedings of CVPR*, 2018, pp. 4510–4520.
- [81] M. Afifi and M. S. Brown, "Deep white-balance editing," in *Proceedings of CVPR*, 2020, pp. 1397–1406.
- [82] G. D. Finlayson, M. Mackiewicz, and A. Hurlbert, "Color correction using root-polynomial regression," *IEEE Trans. Image Process.*, vol. 24, no. 5, pp. 1460–1470, 2015.
- [83] G. Hong, M. R. Luo, and P. A. Rhodes, "A study of digital camera colorimetric characterization based on polynomial modeling," *Color Research & Application*, vol. 26, no. 1, pp. 76–84, 2001.
- [84] Adobe Inc. (2012) Adobe digital negative (dng) specification. [Online]. Available: [https://www.adobe.com/content/dam/acom/en/products/photoshop/pdfs/dng\\_spec\\_1.4.0.0.pdf](https://www.adobe.com/content/dam/acom/en/products/photoshop/pdfs/dng_spec_1.4.0.0.pdf)
- [85] C. Knaus and M. Zwicker, "Progressive image denoising," *IEEE Trans. Image Process.*, vol. 23, no. 7, pp. 3114–3125, 2014.
- [86] T. Mertens, J. Kautz, and F. Van Reeth, "Exposure fusion," in *Proceedings of GRAPP*, 2007, pp. 382–390.
- [87] K. Simonyan and A. Zisserman, "Very deep convolutional networks for large-scale image recognition," *arXiv preprint arXiv:1409.1556*, 2014.
- [88] H. Talebi and P. Milanfar, "Learned perceptual image enhancement," in *Proceedings of ICCP*, 2018, pp. 1–13.
- [89] A. Abdelhamed, S. Lin, and M. S. Brown, "A high-quality denoising dataset for smartphone cameras," in *Proceedings of CVPR*, 2018, pp. 1692–1700.
- [90] Y. Hu, H. He, C. Xu, B. Wang, and S. Lin, "Exposure: A white-box photo post-processing framework," *ACM Trans. Graph.*, vol. 37, no. 2, pp. 1–17, 2018.
- [91] K. Matkovic, L. Neumann, A. Neumann, T. Psik, and W. Purgathofer, "Global contrast factor—a new approach to image contrast," *Computational Aesthetics*, vol. 2005, no. 159–168, p. 1, 2005.
- [92] K. Gu, W. Lin, G. Zhai, X. Yang, W. Zhang, and C. W. Chen, "No-reference quality metric of contrast-distorted images based on information maximization," *IEEE Trans. Cybern.*, vol. 47, no. 12, pp. 4559–4565, 2016.
- [93] K. Dabov, A. Foi, V. Katkovnik, and K. Egiazarian, "Image denoising by sparse 3-D transform-domain collaborative filtering," *IEEE Trans. Image Process.*, vol. 16, no. 8, pp. 2080–2095, 2007.
- [94] H. Talebi and P. Milanfar, "NIMA: Neural image assessment," *IEEE Trans. Image Process.*, vol. 27, no. 8, pp. 3998–4011, 2018.
- [95] B. Jacob, S. Kligys, B. Chen, M. Zhu, M. Tang, A. Howard, H. Adam, and D. Kalenichenko, "Quantization and training of neural networks for efficient integer-arithmetic-only inference," in *Proceedings of CVPR*, 2018, pp. 2704–2713.